applied sciences

MDPI

Article

Study on the Overburden Failure Law of Extra-Thick Coal Seam Mining Under Extremely Thick Conglomerate Strata

Sun Binyang [1,2,3,4,*], Hu Xiongwu [2,3] and Fu Maoru [3]

[1] The Key Laboratory of Mine Geological Disaster Prevention of Anhui Province, Anhui University of Science and Technology, Huainan 232001, China
[2] State Key Laboratory for Safe Mining of Deep Coal Resources and Environment Protection, Huainan 232000, China; hxw_aust@163.com
[3] School of Earth and Environment, Anhui University of Science and Technology, Huainan 232001, China; fumaoru850728@aust.edu.cn
[4] Anhui Huizhou Geology Security Institute Co., Ltd., Hefei 231202, China
* Correspondence: bysun_1993@163.com

Abstract

This study investigates the mining-induced overburden failure and the development law of the water-conducting fracture zone under key layer control during the extraction of an extra-thick coal seam (thickness $\geq$ 8 m) under extremely thick conglomerate strata (thickness $\geq$ 200 m) in the Zhaoxian Coal Mine, Binchang mining area, Shaanxi Province, China. A combined approach utilizing FLAC^{3D} numerical simulation and ground borehole full-section resistivity monitoring was adopted. The results indicate that the primary key layer (extremely thick conglomerate) and the sub-key layer (sandy mudstone) exert a significant inhibitory and segmented control effect on fracture development. The height of the water-conducting fracture zone increases in a "step-like" pattern with working face advancement, stabilizing at 270.3 m; the $R_{h/m}$ is 23.5. The overburden failure morphology evolves dynamically through stages described as "funnel shape–concave shape–inverted trapezoid shape" as mining progresses. Field resistivity monitoring results (fracture zone height of 255 m, $R_{h/m}$ of 22.17) show good agreement with numerical simulations, validating the control mechanism of key layers on overburden failure. These findings provide a theoretical basis for safe mining practices and water resource protection in extra-thick coal seams overlain by extremely thick conglomerate strata.

Keywords: extremely thick conglomerate; extra-thick coal seam; overburden failure; fracture development; borehole full-section resistivity

Check for updates

Received: 19 January 2026
Revised: 16 February 2026
Accepted: 21 February 2026
Published: 24 February 2026

Copyright: © 2026 by the authors. Licensee MDPI, Basel, Switzerland. This article is an open access article distributed under the terms and conditions of the Creative Commons Attribution (CC BY) license.

1. Introduction

China's energy resource endowment is characterized by a relative scarcity of oil and gas but an abundance of coal, which determines that coal will maintain its dominant role in the national energy structure in the short term. As a fundamental energy source, coal is of strategic importance to national energy security. Consequently, the strategic focus of coal development is accelerating its shift toward western regions [1]. Currently, the annual output from Shanxi, Shaanxi, Inner Mongolia, Ningxia, and Xinjiang already accounts for over 80% of the national total. It is projected that by 2035, the share of output from western mining areas will further increase to 90% [2]. In terms of resource occurrence, thick coal seams (thickness $\geq$ 3.5 m) constitute approximately 45% of national reserves and represent

the primary mining targets. Among these, extra-thick coal seams (thickness $\geq$ 8 m) account for over 50% of thick seam reserves, occupying a prominent position in the resource structure. However, the mining of thick and extra-thick coal seams—owing to the large extraction space and intense mining-induced disturbances—can readily damage the structure of key aquicludes, leading to serious ecological and environmental problems. Therefore, investigating the failure mechanisms of subsurface strata and the development of water-conducting fractures under the control of key strata is crucial for achieving coordinated safe mining of thick and extra-thick coal seams and the protection of water resources [3–6].

Mining-induced fractures in overburden are a primary factor that damages key aquifer structures and affects surface ecology. Consequently, studying the development laws of mining-induced fractures and their influencing factors has become a key focus in coal mining research [7]. In particular, predicting the development height of the water-conducting fracture zone has long attracted extensive attention from scholars worldwide. In China, predictions have historically relied on empirical formulas from the "Regulations for Coal Pillar Retention and Mining Under Buildings, Water Bodies, Railways and Main Shafts" (the "Three Under" regulations), which are based primarily on mining height and overburden strength. However, extensive mining practice indicates that these formulas are no longer adequate for the ultra-wide and ultra-thick mining conditions prevalent in modern coal bases such as Huanglong [8]. Currently, scholars employ theoretical calculations, field monitoring, and numerical simulation methods to study overburden fracture laws induced by coal mining [9,10]. Among these, numerical simulation provides an effective, low-cost means to accurately reconstruct roof movement and fracturing during coal extraction, enabling precise prediction of overburden failure height.

Commonly used simulation methods for mining-induced overburden movement and fracturing include the finite element method (FEM), finite difference method (FDM), and discrete element method (DEM), implemented in software such as ANSYS, ABAQUS, FLAC, and UDEC. These methods utilize constitutive models such as ideal elastoplastic, strain-softening plastic, and elastoplastic damage to calculate stress evolution and employ strength criteria (e.g., Mohr–Coulomb, Mises) to assess overburden failure states based on plastic zones, damage zones, and energy zones [11,12]. For instance, XU et al. (2023) analyzed the deformation mechanism above a goaf in Jingmen Garden Expo Park using FLAC3D numerical simulation to evaluate goaf stability, assess site suitability, and explore ecological restoration models [13]. WANG et al. (2025) based on FLAC, discussed complex overburden fracture movement and mining pressure evolution when an inclined lower mining face passes through residual upper coal pillars during slice mining of an extremely thick coal seam [14]. LE et al. (2025) investigated the mechanism of longwall mining-induced roof weighting and its interaction with shield support and coal wall stability using a panel-scale DEM model calibrated with real-time monitoring data [15]. LI et al. (2022) used UDEC to analyze mountain deformation in response to underground mining, finding that mining accelerates overburden fracturing and forms stepped through-sliding surfaces [16]. WANG et al. (2022) employed UDEC with fluid–solid coupling to study overburden movement and surface subsidence at the Daojiao Coal Mine [17]. XU et al. (2025) used UDEC 7.0 to explore fracture development at the Dongxia Coal Mine, finding that the fracture zone height followed an S-shaped curve with face advancement [18]. LE and VU (2025) investigated the floor stress distribution under coal pillars and roadway stability in close-distance coal seams at Thong Nhat Coal Mine through FLAC^{3D} numerical modeling [19]. These studies have provided important references for understanding the evolution of the mining-induced stress field and the control effect of key layers. However, current research still pays insufficient attention to the fracture control mechanism of special geological features such as extremely thick conglomerate strata.

In summary, existing research on mining-induced fracture development predominantly focuses on engineering factors such as working face size, mining height, and mining speed, while relatively insufficient attention is paid to key geological characteristics such as overburden sedimentary structure, lithological combination, and geological structure. In particular, the fracture control mechanism and breaking patterns when extremely thick conglomerate strata serve as the primary key stratum have not yet been systematically understood. Therefore, based on the geological prototype of the typical overburden sedimentary characteristics at the Zhaoxian Coal Mine (Binchang mining area, Huanglong coal base), this study employs the FLAC^{3D} numerical simulation method to analyze the influence of extremely thick conglomerate strata on the development pattern of mining-induced fractures in overburden. It clarifies the characteristics of overburden fracture and fracture field evolution in deep, extra-thick coal seams under such conglomerate coverage and conducts in situ borehole full-section resistivity monitoring. The research findings are not only crucial for water-conservation mining in China's western mining regions but also provide universal theoretical references and practical insights for preventing roof water inrush hazards and optimizing support design under similar geological conditions worldwide.

2. Geological Conditions and Characteristics of the Study Area

The study area, the Zhaoxian Mine Field, is located within Zhaoxian Town, Baoji City, Shaanxi Province (Figure 1a). It belongs to the Binchang mining area of the Huanglong coal base and primarily mines Jurassic coal seams. Owing to geological tectonic effects, some strata are missing in the first mining district of the Zhaoxian Mine Field. Overall, ten stratigraphic groups from the Quaternary, Cretaceous, and Triassic systems are developed. A schematic comprehensive lithological column is shown in Figure 1b. According to 3D seismic data, folds and faults are the main structural features in the mining district, although the overall structure is relatively simple.

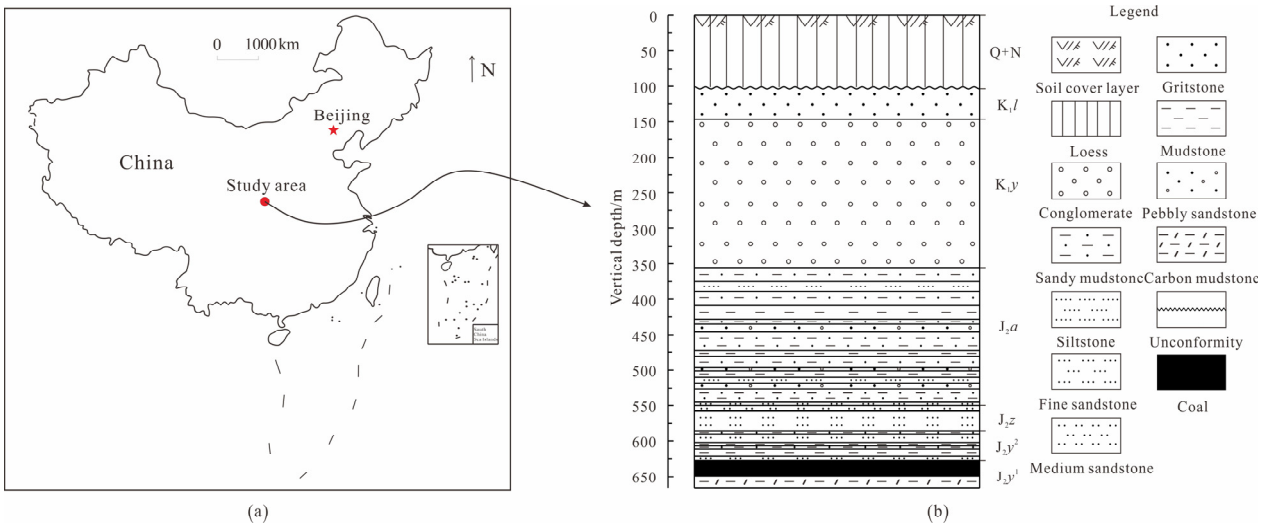

Figure 1. Geographical location and stratigraphic distribution of the study area. (**a**) Geographical location map of the study area; (**b**) Schematic diagram of lithological distribution of strata in the study area.

Based on lithological data from boreholes in the first mining district (covering five working faces: 1302, 1304, 1303, 1305, and 1307), the thickness of each stratum was statistically compiled, as shown in Figure 2. Combined with Figure 1b, it is concluded that the overburden in the Zhaoxian Mine Field is mainly composed of conglomerate (K_1y), sandy mudstone (J_2a, J_2z), mudstone (J_2a, J_2z), and sandstone (K_1l, J_2a, J_2z). Among these,

the Yijun Formation contains extremely thick conglomerate strata (K_1y), with an average thickness reaching 186 m, which plays a significant controlling role in overburden movement. In the first mining district of Zhaoxian Coal Mine, the No. 3 coal seam is located approximately 250 m below the thick sandy conglomerate aquifer of the Cretaceous Yijun Formation. The Luohe Formation has an average thickness of 30 m; the No. 3 coal seam averages 13 m in thickness; the Anding Formation, primarily composed of argillaceous rocks, averages 167 m in thickness; and the Zhiluo and Yan'an Formations are weakly water-rich aquifers with a combined average thickness of 53 m. The specific yield of boreholes in the Yijun Formation ranges from 0.0061 to 0.03796 L/(s·m), classifying it as weakly water-rich. However, due to its great thickness and substantial static reserves, it is prone to forming bed separation water spaces through differential subsidence deformation with the underlying argillaceous rocks of the Anding Formation. The problem of high-level bed separation water inrush involves hydrogeology, engineering geology, mining engineering, and rock mechanics. Its formation mechanism is complex, and prevention and control measures are challenging. The issue of high-level bed separation water carrying mud and sand inrush further complicates the problem, and current research on this topic remains limited both domestically and internationally. Therefore, detailed studies on overburden conditions in the first mining district of Zhaoxian Coal Mine are necessary. This includes research on the mechanism of compound disasters involving strong strata pressure and mud/sand-carrying water inrush, the interaction between strata pressure management and water hazard prevention, and the technical systems for compound disaster prevention and control.

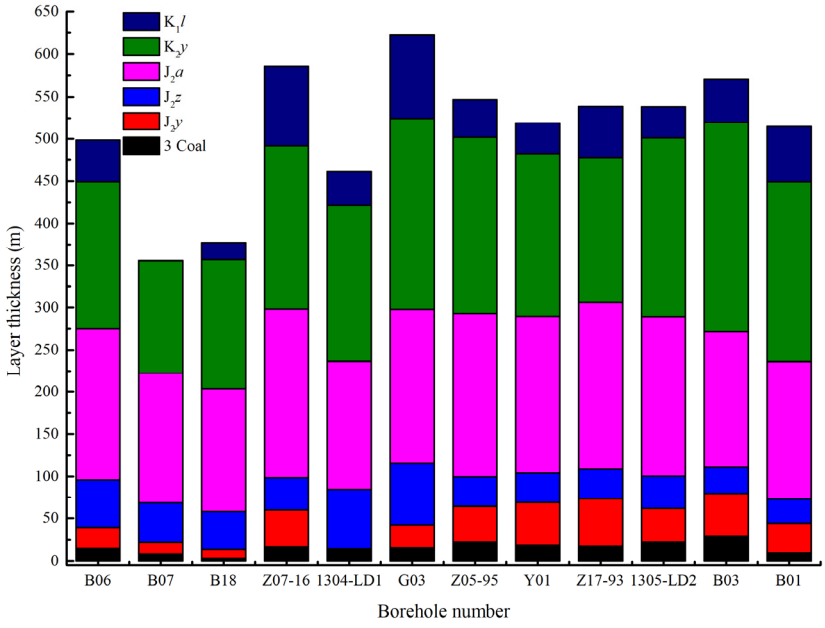

Figure 2. Schematic diagram of the statistical distribution of borehole strata thickness.

3. Model Construction Process

3.1. Selection of Case Study

Based on the revealed lithological characteristics and geological distribution patterns from boreholes, the main mining coal seam (No. 3) in Zhaoxian Coal Mine has a relatively large burial depth of approximately 630 m, with a complete stratigraphic structure. The overburden soil–rock structure above the coal seam represents a widely distributed basic structural type in the study area, "sand layer—soil layer—conglomerate layer—sandy mudstone layer," making it representative. The 1305 working face of Zhaoxian Coal Mine is located in the central part of the mining district, with a strike length of 1000 m, a dip

width of 200 m, and a coal seam dip angle ranging from 5° to 18° (average about 12°). The coal seam thickness ranges from 11.1 to 23.0 m, averaging 16.2 m, with an actual mining thickness of 11.5 m. Geologically representative of the mining area, this working face features a complete overburden sequence characterized by the typical "soil layer–conglomerate–sandy mudstone" structure. Its mining parameters, such as depth and seam thickness, fall within the median range of the mine's conditions, ensuring that the research findings possess broad applicability across the mining district. The preferred mining method for the No. 3 coal seam is fully mechanized top-coal caving. Borehole logging curves from the 1305 working face indicate that approximately 269 m above the No. 3 coal seam roof, there exists a conglomerate layer of 208 m thickness (K_1y), whose mechanical properties differ significantly from those of other rock layers. This paper takes the 1305 working face as the study object, employing the finite difference method for simulation to analyze the characteristics and laws of mining-induced fracture development in deep, extra-thick coal seams under extremely thick conglomerate coverage.

3.2. Model Construction

Using the occurrence conditions of the No. 3 coal seam in Zhaoxian Coal Mine as the geological prototype, and based on the principle of "grasping key points, retaining characteristics, reasonably simplifying, and approximating the prototype," the overburden structure in the numerical model was designed as "sand layer—soil layer—conglomerate layer—sandy mudstone layer—coal seam". The model's geometric dimensions were set as follows: length 1200 m, width 400 m, and height 656 m. The thickness of the No. 3 coal seam is 11.5 m.

Key information, such as overburden categories and layer thickness, was obtained from the comprehensive columnar section of the coal seam roof and floor in the 1305 working face. The surface cover consists of loess and sandy soil. The coal seam roof comprises mudstone, sandy mudstone, sandstone, conglomerate, etc. The physical and mechanical parameters of the strata were input into key layer discrimination software [20], identifying the extremely thick conglomerate of the Yijun Formation (layer thickness 208 m) as the primary key layer and the sandy mudstone of the Anding Formation (layer thickness 53.45 m) as the sub-key layer. The basic physical and mechanical parameters for each rock layer were obtained from laboratory mechanical tests and geological borehole lithology test reports, as detailed in Table 1.

Table 1. Summary of rock mechanical parameters used in numerical simulation.

Group	Lithology	Unit Weight (kg/m^3)	Tensile Strength (MPa)	Cohesion (MPa)	Internal Friction Angle (°)	Bulk Modulus ($\times 10^4$ MPa)	Shear Modulus ($\times 10^4$ MPa)
Q + N	Loess	1380		1	30	0.25	0.115
K_1l	Fine Sandstone	2456	1.25	1.57	31	0.628	0.395
K_1y	Conglomerate	2585	8.37	13.155	39	2.146	1.746
J_2a	Sandy Mudstone	2455	0.655	1.15	38.09	0.552	0.315
	Fine Sandstone	2405	1.085	1.69	34.245	0.640	0.441
	Siltstone	2455	0.97	2.225	30.665	0.580	0.365
	Mudstone	2490	1.04	3.195	37.365	0.761	0.413
	Gravel-bearing sandstone	2345	0.175	0.555	37.87	0.528	0.348
	Sandy Mudstone	2455	1.005	2.995	34.1	0.833	0.524
J_2z	Fine Sandstone	2471	1.6	2.625	33.54	0.786	0.541
	Sandy Mudstone	2615	1.705	2.3	37.29	1.336	0.940
	Medium Sandstone	2410	0.73	2.655	34.335	0.712	0.448

Table 1. *Cont.*

Group	Lithology	Unit Weight (kg/m^3)	Tensile Strength (MPa)	Cohesion (MPa)	Internal Friction Angle (°)	Bulk Modulus ($\times 10^4$ MPa)	Shear Modulus ($\times 10^4$ MPa)
J_2y	Sandy Mudstone	2496	0.945	2.02	33.685	0.882	0.634
	Fine Sandstone	2450	1.73	4.085	36.375	0.997	0.764
	Mudstone	2576	1.215	3.64	33.025	0.651	0.419
	No. 3 Coal	1330	0.74	3.2	34.48	0.428	0.232
	Carbon Mudstone	2576	0.34	2.36	31.18	0.615	0.387

This study employs the Mohr–Coulomb elastic–plastic constitutive model [21]. Although conglomerate rock is heterogeneous, in large-scale engineering simulations, its macroscopic mechanical behavior (such as shear failure) can be equivalently characterized by the strength parameters (cohesion and internal friction angle) of this criterion. This model effectively reflects the shear slip and the plastic zone development of the rock mass under mining conditions and is a classic model widely used in geotechnical engineering. The specific form of the model is as follows:

$$f_s = (\sigma_1 - \sigma_3)(1 + \sin\alpha)/(1 - \sin\alpha) - 2c\sqrt{(1 + \sin\alpha)/1 - \sin\alpha} \quad (1)$$

In Equation (1), σ_1 represents the maximum principal stress, σ_3 represents the minimum principal stress, c represents the cohesion, and α represents the internal friction angle.

The numerical model of the 1305 working face is shown in Figure 3. Based on the initial equilibrium model, coal seam extraction was simulated. The mining face advances stepwise from right to left along the x-direction. A 200 m protective coal pillar was reserved on each side of the open-off cut, and a 100 m wide protective coal pillar was reserved on each side along the dip direction. Each mining step extracted 40 m of the coal seam, totaling 20 extraction steps. The influence of composite key layer control conditions on the development characteristics and laws of mining-induced fractures was simulated and analyzed.

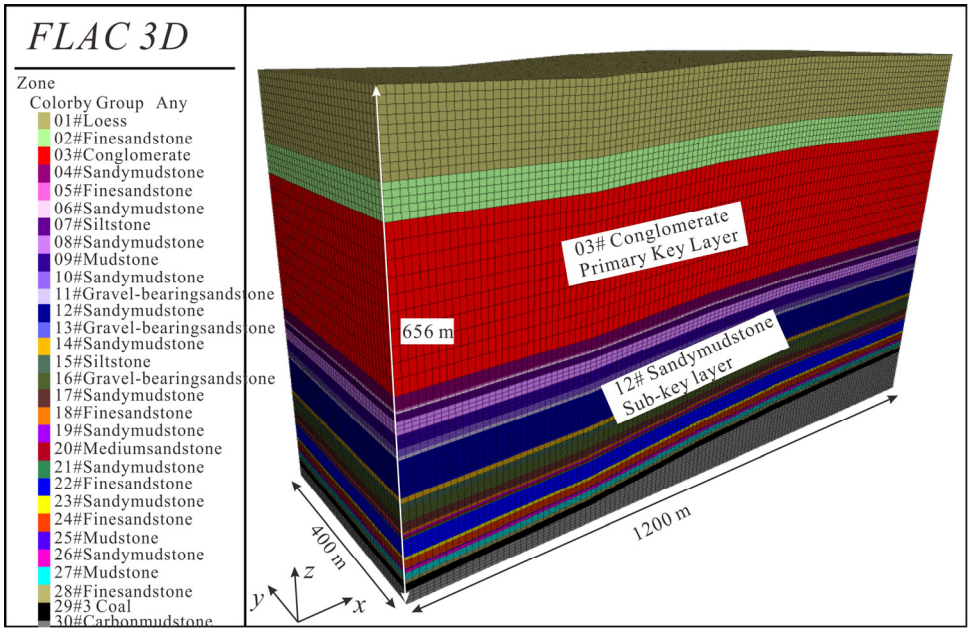

Figure 3. Schematic diagram of the 3D numerical simulation model of the 1305 working face.

4. Analysis of Numerical Simulation Results

4.1. Development Process of Mining-Induced Fractures in Overburden

The numerical simulation primarily analyzed the characteristics of mining-induced fracture development through the distribution of the plastic zone in the middle longitudinal section along the strike of the working face. Figure 4 shows the evolution characteristics of overburden fracture and movement. As the mining distance increases, the roof strata undergo processes such as sagging, loss of integrity, fracturing, and gradual subsidence.

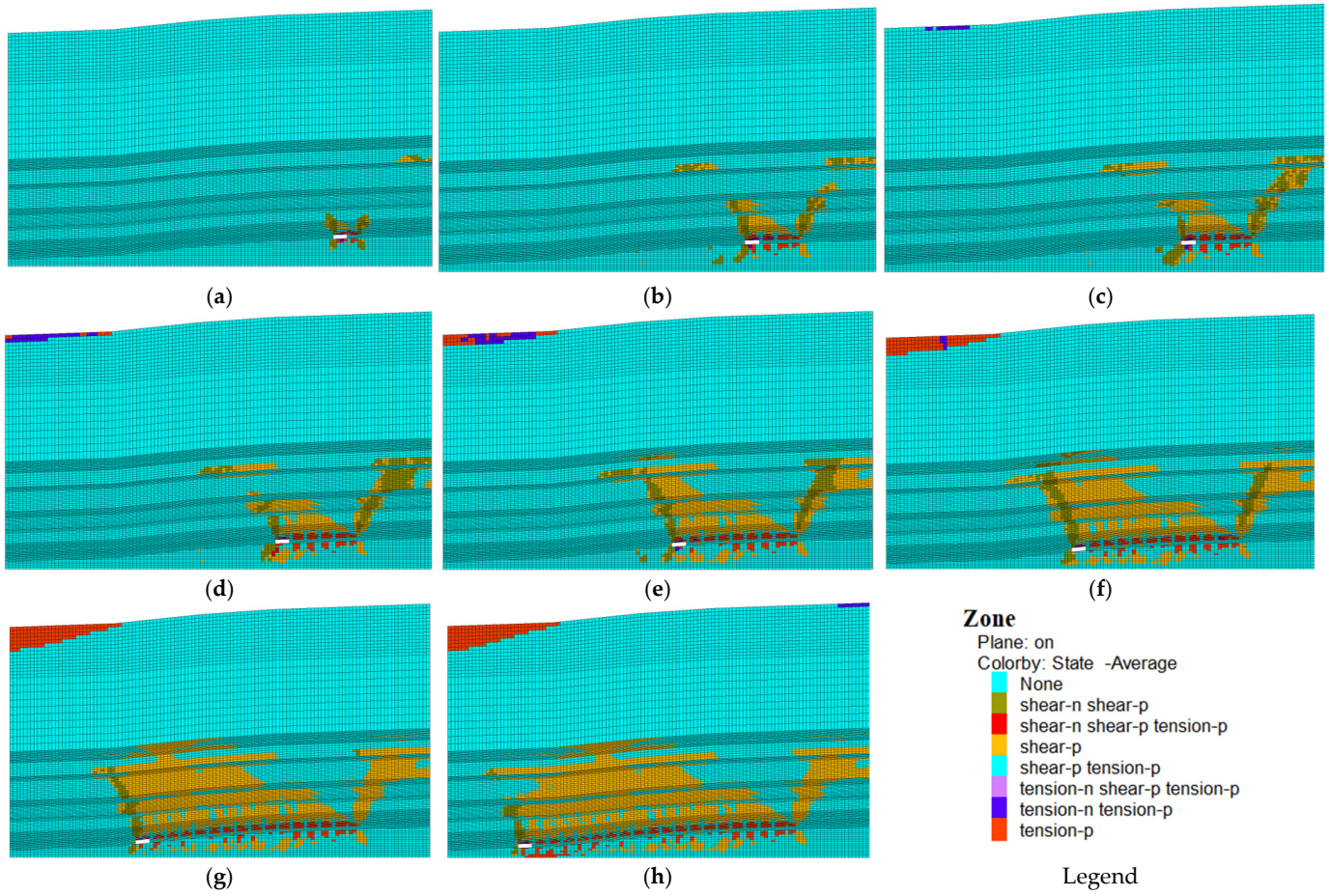

Figure 4. Distribution and development characteristics of the overburden failure plastic zone. (**a**) Excavation at 80 m; (**b**) excavation at 160 m; (**c**) excavation at 200 m; (**d**) excavation at 240 m; (**e**) excavation at 360 m; (**f**) excavation at 480 m; (**g**) excavation at 560 m; (**h**) excavation at 800 m.

When the coal seam is mined for 40 m (Figure 4a), tensile failure occurs in the immediate roof and floor, while shear failure is observed above the open-off cut and the working face. The presence of the plastic zone indicates partial deformation and failure in these areas. Based on the continuity of plastic zone distribution, the fine sandstone and mudstone of the immediate roof are considered to undergo overall caving, manifested as tensile failure—characteristic of the caved zone. The shear failure zone primarily constitutes the water-conducting fracture zone.

When mining reaches 160 m, the vertical extent of the overburden plastic zone expands further. Mining-induced fractures above the open-off cut develop upward first. However, due to the short-term load-bearing effect of the sub-key layer (No. 12 sandy mudstone), overall mining-induced fractures extend and develop forward along the bottom of this sandy mudstone layer. Vertically, fracture development shows stagnation. The overall

fracture development morphology resembles a "funnel shape". Similar characteristics are observed when mining reaches 200 m and 240 m.

When mining reaches 280 m, fractures above the open-off cut gradually develop upward into the No. 12 sandy mudstone layer. By 360 m, fractures directly above the working face also develop into this layer, and the overburden above the central part of the goaf are considered to have fractured into the sandy mudstone. At this stage, the overall overburden mining-induced fractures exhibit a "concave shape" development characteristic, with higher ends and a lower middle.

As mining continues, the plastic zone of overburden fractures continues to increase. However, owing to the load-bearing effect of the No. 12 sandy mudstone, the main body of the plastic zone develops within it and the lower strata, while the plastic zone in the upper strata mainly develops above the working face end, as shown in Figure 4f,g.

When mining reaches 800 m (extraction completed), overburden fracture development has essentially stabilized. Constrained by the main controlling effect of the primary key layer (No. 3 conglomerate), overburden fractures barely develop into the conglomerate interior, affecting only about 0.7 m at the bottom interface. The overall morphology of mining-induced overburden fractures is an "inverted trapezoid shape". The plastic zone distribution is highest in the middle of the goaf. Development above the open-off cut end was rapid initially but later occurred mainly in strata above the working face end.

In summary, during the coal seam mining process, the overall morphology of mining-induced fracture development within the overburden presents a dynamic evolution sequence: "funnel shape—concave shape—inverted trapezoid shape". The analysis suggests that the main reason is the delayed movement, deformation, and caving of the overburden during coal seam extraction, which imparts distinct stage characteristics to overburden fracture development. Taking the simulation of coal seam extraction in the 1305 working face as an example, in the early stage, mining-induced fractures in the overburden are influenced by the sub-key layer, initially developing laterally along the bottom of the sandy mudstone. When the mining-induced fractures penetrate the interior of the sandy mudstone, the overburden plastic zone develops upward into the upper part of the sub-key layer and gradually expands. In the later stage, constrained by the main controlling effect of the primary key layer—the extremely thick conglomerate—overburden fractures only develop along the bottom interface of the conglomerate layer. Until mining is completed, they do not penetrate into the interior of the conglomerate layer, affecting only about 0.7 m at its bottom interface. It is also evident that, owing to the load-bearing effect of the extremely thick conglomerate in the Anding Formation during the extraction of the No. 3 coal seam, the surface damage and subsidence range is small, with only part of the surface in front of the stopping line exhibiting certain tensile failure characteristics.

4.2. Development Height of Mining-Induced Fractures in Overburden

After extraction, the overburden undergoes movement, deformation, and caving, leading to the development of horizontal and vertical fractures, thus forming the caved zone, fracture zone, and bed separations. The development height of the water-conducting fracture zone after each mining step was manually extracted from the plastic zone distribution contour in the longitudinal section. The growth rate was then calculated as the incremental height increase per 40 m of face advance, as shown in Figure 5.

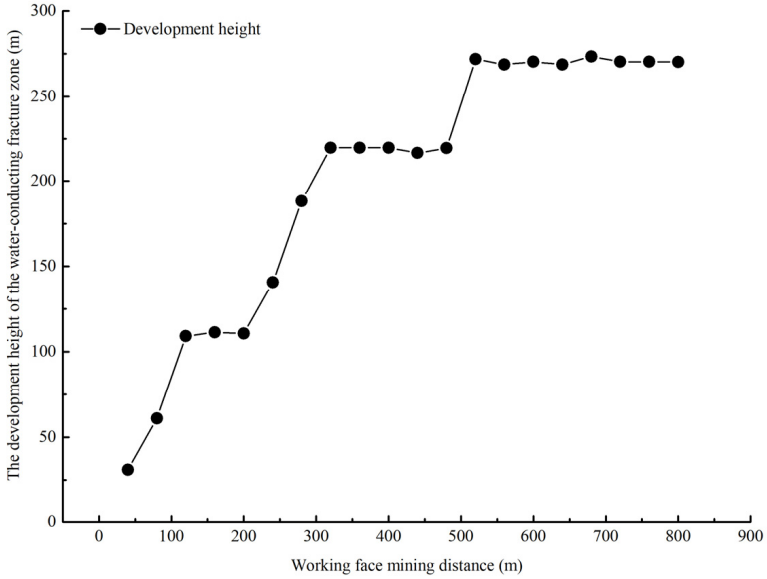

Figure 5. Statistical evolution of water-conducting fracture zone height with working face advance.

As seen in Figure 5, with working face advance, mining-induced fractures continuously increase. When mining advances from 40 to 120 m, fracture height increases linearly with advance; the vertical growth rate is approximately 1 (i.e., fracture height increase per unit advance is equivalent). At 120 m, the fracture top interface reaches the bottom of the sub-key layer (No. 12 sandy mudstone). Owing to its control effect, when mining reaches 200 m, fractures do not extend vertically (growth rate 0). From 200 to 320 m, fractures penetrate the sandy mudstone, leading to upward development (growth rate returns to 1). The plastic zone top interface then reaches stronger layers above the sandy mudstone. Controlled by the incomplete fracture of the sandy mudstone and the higher bearing capacity of upper strata, the plastic zone top does not rise when mining reaches 480 m (growth rate 0). From 480 to 520 m, fractures develop upward near the bottom interface of the extremely thick conglomerate (K_1y). After mining completion, the plastic zone height does not expand significantly, demonstrating the pronounced inhibitory effect of the conglomerate on vertical fracture development.

In summary, under composite key layer control, the water-conducting fracture zone height during simulated extraction of the No. 3 coal seam increases in a "step-like" manner. Under the control of the sub-key layer (sandy mudstone) and primary key layer (conglomerate), fracture development exhibits a step-like characteristic upon reaching the bottom interfaces of these strata. Numerical simulation indicates a final water-conducting fracture zone height of 270.3 m for the 1305 working face. With a mining height of 11.5 m, the ratio of the height of the water-conducting fracture zone to the mining thickness of the coal seam ($R_{h/m}$) is 23.5.

4.3. Movement Law of Mining-Induced Overburden

After extraction, the original stress state of the overburden is disrupted. As the goaf expands, strata within a certain range above the roof undergo movement, deformation, and caving. Vertical displacement (settlement) was monitored at a series of virtual measurement points embedded within different rock layers along the model's central line. Figure 6 shows settlement curves for monitoring points within various overburden at different mining distances (120 m, 240 m, 360 m, 480 m, 720 m, and 800 m).

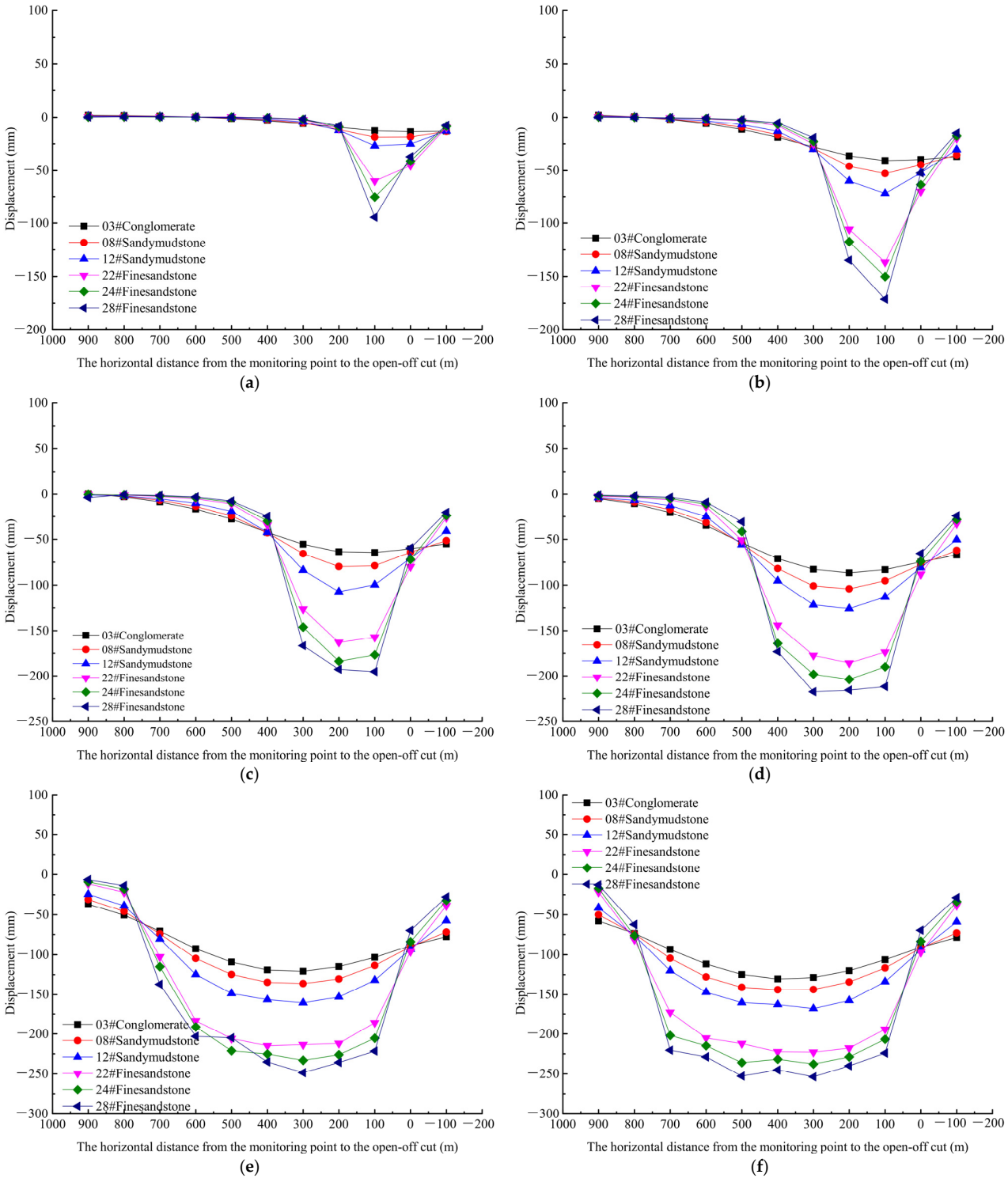

Figure 6. Settlement curves of monitoring points during the working face advance. (**a**) Excavation at 120 m; (**b**) excavation at 240 m; (**c**) excavation at 360 m; (**d**) excavation at 480 m; (**e**) excavation at 720 m; (**f**) excavation at 800 m.

When mining reaches 120 m (Figure 6a), the immediate roof bends and fractures, forming a mechanical state characterized by hinged ends and a subsided middle. The middle portion is partially supported by caved rock fill, causing the immediate roof monitoring line to present a "V-shaped" subsidence morphology, which is largely symmetrical.

As the working face advances, the lateral span of the goaf increases, the key layer undergoes periodic fracture and subsidence, and rock layers in the caved zone gradually

become compacted. At 360 m, overburden subsidence morphology gradually transitions to "U-shaped".

Comparing Figure 6e,f, when mining reaches 720 m, settlement of each rock layer above the roof has essentially stabilized. During subsequent extraction, subsidence morphology only expands laterally, without further vertical development. After completion, the overall subsidence morphology of the stope overburden presents an "inverted trapezoid shape," consistent with the plastic zone distribution morphology.

5. Field Measurement of Overburden Failure Height

5.1. Selection of Measurement Method

The structural characteristics of mine rock mass significantly affect resistivity, and a strong correlation exists between the two. Resistivity values differ for different lithologies. For the same rock layer, changes in its structure also alter resistivity. For coal seam roof strata, electrical property analysis shows coal has relatively high resistivity, sandstone exhibits intermediate values, and clay rocks display the lowest resistivity. When rock layers undergo deformation and failure, if dry, conductivity deteriorates and local resistivity increases; if water-bearing, conductivity improves, manifesting as a local low-resistivity. Changes in the electrical properties of rock layers in both vertical and horizontal directions during mining reflect their failure and fracture development [22]. Therefore, analyzing deformation and failure laws by testing resistivity changes at different depths provides the geological basis for electrical methods to assess overburden failure characteristics [23].

The development of the water-conducting fracture zone manifests as resistivity changes in rock layers below a certain height. Each test uses the background resistivity distribution as a baseline. Dynamic testing can intuitively analyze the failure process and laws from a spatiotemporal perspective. A sudden decrease in resistivity across the entire profile can also indicate the possibility of water hazards in the overburden.

5.2. Layout of Measurement Borehole

To determine overburden failure height, fracture development morphology, and disturbance to the extremely thick conglomerate during mining of the 1305 working face, one mining response monitoring borehole (1305-LD1) was installed on the surface (Figure 7). The borehole is located 737 m from the open-off cut and 53 m from the transporting roadway. Its bottom is about 15 m above the No. 3 coal seam roof; its diameter is Φ133 mm, and its depth is −610 m. High-density resistivity sensor units are installed inside. Each electrode unit is packaged in parallel and operates independently, enabling point-line-surface integrated measurement. They possess good mechanical tensile/compressive strength and high stability.

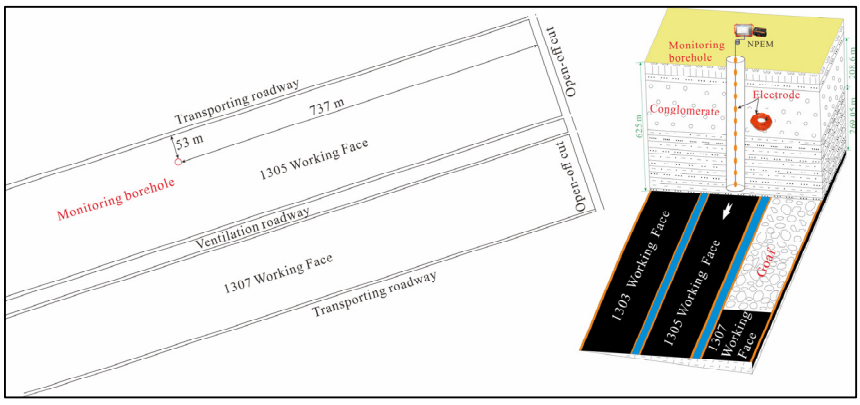

Figure 7. Layout of borehole and installation of sensor units.

5.3. Measurement System and Data Acquisition

A high-density resistivity sensor array was installed in borehole 1305-LD1 prior to the mining activity to establish a background resistivity profile. Measurements were taken at 24 h intervals throughout the entire mining period of the 1305 working face. The system recorded apparent resistivity data across the full borehole depth, enabling time-lapse monitoring of geoelectrical changes induced by mining.

5.4. Analysis of Overburden Failure Measurement Results

A total of 80 sets of electrical data were collected. Several representative resistivity profiles were selected for analysis. Figure 8 shows a schematic of the correspondence between some borehole apparent resistivity profiles and strata. Apparent resistivity in the monitoring hole is represented by a color scale from cool to warm tones, corresponding to 0 to 490 Ω·m, respectively.

As shown in Figure 8, apparent resistivity distribution aligns well with the geological profile, and values differ significantly between layers. The middle and lower parts of the extremely thick conglomerate (K_1y) exhibit relatively high apparent resistivity, while sandy mudstone and mudstone sections show lower values, consistent with physical property differences. This indicates good data quality, suitable for subsequent analysis.

When the working face is ahead of the borehole (Figure 8a), the overburden remains relatively intact without major fractures. Influenced only by abutment pressure, the resistivity of some layers (e.g., Luohe Formation coarse sandstone and Anding Formation sandy mudstone and mudstone) decreases moderately.

When the working face is behind the borehole (Figure 8b), the coal seam overburden undergoes various strata movements. Instability of the sub-key layer causes bed separation, rotation, fracture, and caving of strata below the primary key layer. The resistivity of the borehole surrounding rock shows local increases or decreases. Immediately after the face passes the borehole (0 to −22 m), surrounding rock integrity remains good. Subsequently, owing to immediate roof caving, the overburden deforms and fails, forming a stress concentration zone, leading to an increase in resistivity.

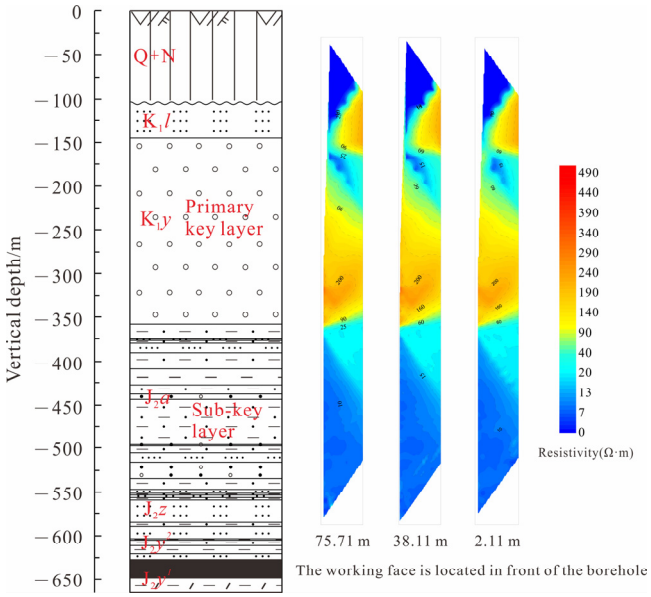

(**a**)

Figure 8. *Cont.*

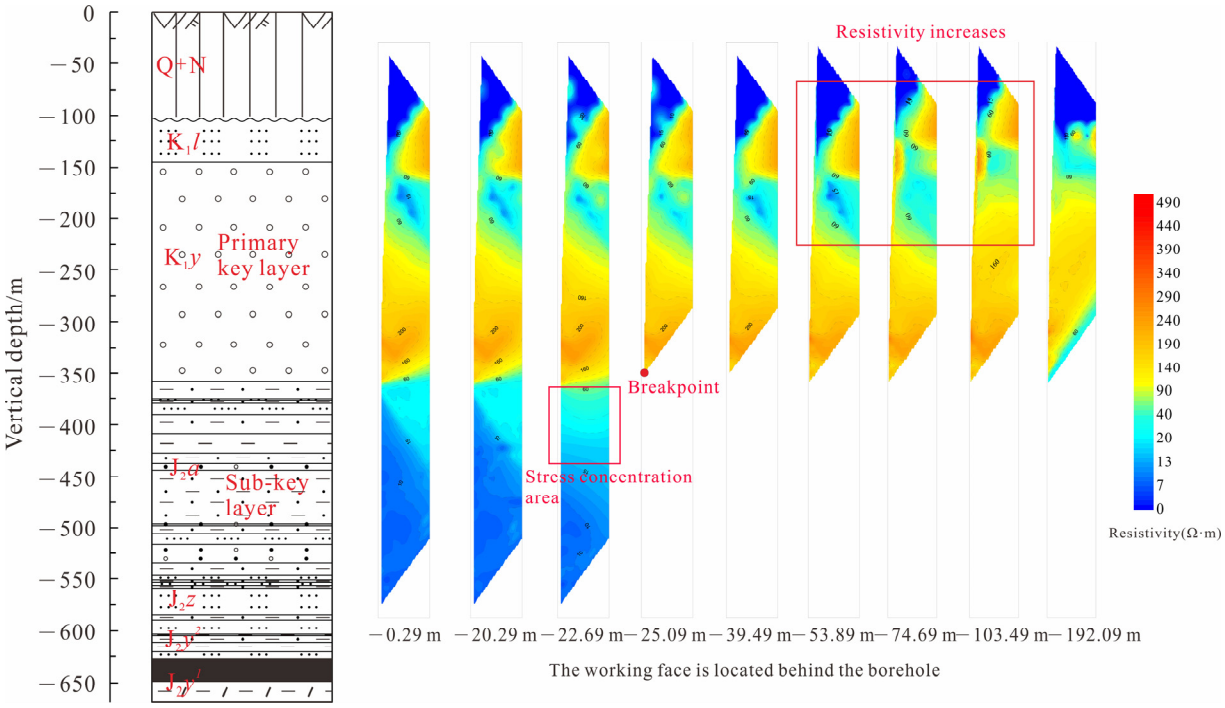

(**b**)

Figure 8. Full-process rock resistivity response characteristics during working face mining. (**a**) Resistivity response when the working face is ahead of the borehole; (**b**) resistivity response when the working face is behind the borehole.

As the working face advances further, overburden deformation intensifies, forming large fractures such as bed separations, which cause shearing of borehole cables and create breakpoints. A breakpoint is located near the boundary between the Yijun Formation conglomerate and the Anding Formation sandy mudstone (−255 m). The resistivity of the conglomerate above this point shows little change, indicating overall relative stability without major deformation.

When the working face passes the borehole from −50 m to −100 m, the resistivity of the middle/lower Yijun Formation conglomerate remains relatively stable, while resistivity from burial depth 0 to −200 m increases significantly. Analysis suggests this is mainly due to fracture development at the interface between the Luohe Formation sandstone and the Yijun Formation conglomerate.

When the working face advances to approximately −200 m, the resistivity inside the borehole decreases. The loess cover (0 to −100 m) shows relatively uniform electrical characteristics with apparent resistivity below 10 Ω·m. The resistivity of the sandstone in the Luohe Formation (−100 to −150 m) and the conglomerate in the Yijun Formation (−150 to −300 m) generally decreased by 10 to 30 Ω·m, indicating that overburden movement has stabilized.

5.5. Analysis of the Development Height of the Overburden Fracture Zone

Comparative analysis of the resistivity distribution maps suggests that, influenced by mining, advance bed separation development is primarily horizontal. Bed separations develop forward along interfaces between different lithologies or weak interfaces within the same lithology. Between periodic roof weighting intervals, advance bed separation continues to develop slowly with minor or gradual resistivity changes. During periodic weighting, advance bed separation fractures are most developed, and resistivity increases suddenly. After main roof periodic weighting and caving, mining-induced stress is released,

advance bed separation fractures partially close, and resistivity decreases. Subsequently, the influence of a new cycle of mining-induced stress increases. After the bed separation zone forms, as the face advances toward it, the fracture range expands and interconnects, forming the water-conducting fracture zone.

Based on typical resistivity characteristics in the overburden water-conducting fracture zone (Figure 8) and regional geology, the analysis concludes that the borehole resistivity profile aligns well with the geological profile, with significant differences between layers (e.g., high resistivity in the middle/lower conglomerate, lower in sandy mudstone/mudstone). This confirms good data quality. When the working face is ahead, the overburden is intact with minor resistivity changes. When the working face is behind, the overburden undergoes strata movement, and sub-key layer instability causes bed separation, rotation, fracture, and caving of strata below the primary key layer. Borehole surrounding rock resistivity shows local increases or decreases. For a period after the working face passes the borehole, surrounding rock integrity remains good. Subsequently, due to immediate roof caving, overburden deformation and failure form a stress concentration zone, causing resistivity to increase. After mining the No. 3 coal seam, the development height of the water-conducting fracture zone reaches 255 m, located at the sandy mudstone layer at the top of the Anding Formation. Calculated with an average mining thickness of 11.5 m, the ratio of the height of the water-conducting fracture zone to the mining thickness of the coal seam ($R_{h/m}$) is 22.17, which is essentially consistent with the numerical simulation results, and the field measurement results are more comprehensive.

6. Discussion and Further Research

This study, through numerical simulation and on-site monitoring, confirmed that extremely thick conglomerate strata serve as the primary key layer and exert strong control over the subsidence height of overburden and the vertical propagation of mining-induced fractures.

The identified step-like development pattern of the water-conducting fracture zone provides critical insights for mine hazard prevention and water-preserved mining. The specific insights are as follows: ① The pronounced inhibitory effect of the extremely thick conglomerate on fracture propagation (only 0.7 m disturbance at its base) significantly reduces the risk of hydraulic connection between the goaf and overlying loose aquifers. This supports the rational design of safety coal pillars and the determination of optimal stopping line positions. ② Understanding the segmented control behavior of key strata enables more accurate prediction of roof pressure behavior, facilitating the selection of suitable shield support capacities and roof management strategies. ③ The verified fracture-to-mining height ratio ($R_{h/m}$ = 22.17–23.5) under such geological conditions offers a site-specific reference for assessing overburden damage and groundwater protection feasibility in ecologically sensitive western mining areas. ④ The research paradigm combining numerical predictive analysis with in situ geophysical verification is transferable to other coalfields with similar thick conglomerate overburden (e.g., Shendong and Ningdong), providing a robust technical framework for green mining practices.

However, the model simplifies the conglomerate rock as a homogeneous isotropic medium, which differs from the actual non-homogeneity of the conglomerate rock (such as cementation differences and internal weak planes). Future research could consider its internal structure in the model, which might reveal more complex fracture propagation paths and even non-continuous sliding along internal weak planes. This might partially weaken its overall control ability on fractures and affect the details of the “step-like” development pattern.

Moreover, the results of this study are of reference value for mining areas with similar geological conditions, but the coupling influence of factors such as underground water flow field and stress direction needs further research.

7. Conclusions

This study integrated FLAC^{3D} numerical simulation and surface borehole resistivity monitoring to reveal the overburden failure law during extra-thick coal seam mining under the control of an extremely thick conglomerate strata acting as the primary key layer. The main conclusions are as follows:

(1) The overburden failure morphology undergoes staged evolution. The development morphology of mining-induced fractures dynamically evolves with working face advance, following a sequence of "funnel shape—concave shape—inverted trapezoid shape". This process is controlled by the load-bearing capacity and fracture timing of the key layers (the extremely thick conglomerate as the primary key layer and the sandy mudstone as the sub-key layer), visually reflecting the "segmented control" mechanism of key layers on the overburden failure process.

(2) The height of the water-conducting fracture zone develops in a "step-like" pattern. Its growth is strongly inhibited at the interfaces of key layers, manifesting as a stepwise pattern of "rapid growth—stagnation—renewed growth". Numerical simulation yielded a final fracture zone height of 270.3 m, with $R_{h/m}$ of 23.5. Field resistivity monitoring results (height of 255 m, $R_{h/m}$ = 22.17) showed good agreement with the simulation, jointly verifying the strong blocking effect of key layers on the vertical propagation of fractures.

(3) The extremely thick conglomerate plays a crucial role in disaster control. As a high-strength primary key layer, the extremely thick conglomerate effectively inhibits the upward connection of fractures to overlying loose aquifers, with only about 0.7 m of disturbance observed at its bottom interface. This provides critical geomechanical evidence for evaluating the risk of roof water hazards under similar geological conditions.

(4) The research methodology is effective and has promotion value. The adopted research paradigm, combining "numerical simulation for predictive analysis" with "in-situ electrical monitoring for dynamic verification", enables accurate and quantitative capture of the entire overburden failure process. It provides a reliable technical approach for achieving water-preserved mining and hazard prevention under similar complex geological conditions.

This study advances the understanding of the overburden failure mechanism in extra-thick coal seam mining under extremely thick conglomerate strata. The findings can provide theoretical support and engineering guidance for coordinating the safe and efficient mining of coal resources with the protection of groundwater systems in ecologically vulnerable mining areas in western China.

Author Contributions: Conceptualization, S.B.; methodology, S.B.; software, H.X.; validation, S.B.; formal analysis, S.B.; investigation, F.M.; resources, S.B.; data curation, S.B.; writing—original draft preparation, S.B.; writing—review and editing, S.B.; visualization, S.B.; supervision, S.B.; project administration, S.B.; funding acquisition, S.B. All authors have read and agreed to the published version of the manuscript.

Funding: This research was funded by the Research Start-up Fund for High-level Introduced Talents of Anhui University of Science and Technology (No. 2023yjrc73); the Open Foundation of the Key Laboratory of Mine Geological Disaster Prevention of Anhui Province (No. 2023-MGDP-02); and the Open Fund of State Key Laboratory for Safe Mining of Deep Coal Resources and Environment Protection (No. 2025YB013).

Data Availability Statement: This study involves field observation data, numerical simulation data, and theoretical calculation data. The data used to support the findings of this study are available from the corresponding author upon request.

Acknowledgments: The authors have reviewed and edited the output and take full responsibility for the content of this publication.

Conflicts of Interest: The authors declare that they have no known competing financial interests or personal relationships that could have appeared to have influenced the work reported in this paper. Author Sun Binyang was employed by Anhui Huizhou Geology Security Institute Co., Ltd. The remaining authors declare that the research was conducted without any commercial or financial relationships that could be perceived as a potential conflict of interest.

Abbreviations

The following abbreviations are used in this manuscript:

$R_{h/m}$	The ratio of the height of the water-conducting fracture zone to the mining thickness of the coal seam

References

1. Wang, S.; Wei, J.; Song, S.; Wang, S.; Sun, T. Influence of thick sandstone on development of overburden mining fissures in northern Shaanxi coal mining area of Yellow River Basin and suggestions on water-preserved coal mining. *Coal Geol. Explor.* **2022**, *50*, 2.
2. Sun, Q.; Zhao, R.; Zhang, J.; Chen, L.; Li, P. The law of overburden failure and water conservation mining method of extra thick coal seams covered by extremely thick soil layers. *J. Min. Saf. Eng.* **2025**, *42*, 1129–1140.
3. Zhang, Y.; Hua, Z.; Song, Y.; Hu, H.; Li, J. Developmental pattern of water flowing fractured zones in the soil-bedrocktype overburden and water-controlled mining strategy under a super-large mining height. *Coal Geol. Explor.* **2025**, *53*, 112–127.
4. Zhang, Y.; Shen, C.; Zhang, Z.; Li, Y. Regional distribution law of water–conducting fractured zone height in high–strength mining of thick and extra–thick coal seams in China. *Coal Sci. Technol.* **2022**, *50*, 38–48.
5. Guo, W.; Zhao, G.; Bai, E. Critical failure of overlying rock strata and its criteria induced by high–intensity longwall mining. *J. China Coal Soc.* **2020**, *45*, 3657–3666.
6. Kang, H.; Li, Q.; Zhang, Y.; Guo, J.; Liu, P. Development status and prospect of green mining and ecological restoration technology of coal mines in China. *J. Green Mine* **2023**, *1*, 1–24.
7. Li, Q.; Li, X.; Xu, J.; Xu, Z.; Zhang, C. Research advances in mining fractures evolution law of rock strata and ecological treatment technology. *Coal Sci. Technol.* **2022**, *50*, 28–47.
8. Zhang, Y.; Zhang, Z. Research progress of mining overlying stratas failure law and control technology. *Coal Sci. Technol.* **2020**, *48*, 85–97.
9. Fan, J.; Yuan, Q.; Chen, J.; Ren, Y.; Zhang, D.; Yao, H.; Hu, B.; Qu, Y. Investigation of surrounding rock stability during proximal coal seams mining process and feasibility of ground control technology. *Process Saf. Environ.* **2024**, *186*, 1447–1459. [CrossRef]
10. Pang, L.; Liu, W.; Zheng, Q.; Du, Y.; Meng, X.; Li, X. Evaluation and analysis of metal mine filling based on numerical simulation and actual measurement. *Environ. Earth Sci.* **2021**, *80*, 505–529. [CrossRef]
11. Wei, J.; Wang, S.; Song, S.; Sun, Q.; Yang, T. Experiment and numerical simulation of overburden and surface damage law in shallow coal seam mining under the gully. *Bull. Eng. Geol. Environ.* **2022**, *81*, 207. [CrossRef]
12. Xu, Z.; Xu, W.; Zhu, Z.; Zhao, J. Research on monitoring and stability evaluation of ground subsidence in gypsum mine goaf. *Front. Environ. Sci.* **2023**, *10*, 1097874. [CrossRef]
13. Xu, Z.; Xu, W.; Zhou, P.; Zhu, Z.; Zhao, J.; Gao, P. Research on Coal Mine Goaf Restoration Based on Stability of Overlying Rocks and Numerical Simulation Analysis: A Case Study of Jingmen Garden Expo Park. *Sustainability* **2023**, *15*, 1464. [CrossRef]
14. Wang, H.; Tian, C.; Liu, Y.; Li, Y.; Lu, M.; Jiao, J.; Bai, J.; Qiao, Z. Overburden structure fracture evolution and ground pressure behavior under oblique residual coal pillars in thick seam mining. *Sci. Rep.* **2025**, *15*, 30932. [CrossRef] [PubMed]
15. Le, T.D.; Nguyen, C.K.; Tran, M.T. Longwall mining-induced weighting mechanism and its interactions with shield support and coal wall. *Min. Miner. Depos.* **2025**, *19*, 1–13. [CrossRef]
16. Li, J.; Li, B.; He, K.; Gao, Y.; Wan, J.; Wu, W.; Zhang, H. Failure mechanism analysis of mining-induced landslide based on geophysical investigation and numerical modelling using distinct element method. *Remote Sens.* **2022**, *14*, 6071. [CrossRef]
17. Wang, Y.; Wu, G.; Liu, Y.; Cheng, Z. Study on overlying strata movement and surface subsidence of coal workfaces with karst aquifer water. *Mathematics* **2022**, *10*, 169. [CrossRef]

18. Xu, J.; Pan, J.; Li, M.; Wang, H.; Chen, J. Dynamic evolution of fractures in overlying rocks caused by coal mining based on discrete element method. *Processes* **2025**, *13*, 806. [CrossRef]
19. Le, Q.P.; Vu, T.T. Numerical modeling analysis of floor stress distribution under coal pillars and roadway stability in close-distance coal seams. *Min. Miner. Depos.* **2025**, *19*, 1. [CrossRef]
20. Li, Z.; Ren, Z.; Du, F.; Ren, H.; Wang, W. Evolutionary pattern and control technology of mine pressure when mining face for coal pillars in main roadways passing through abandoned roadways. *Coal Geol. Explor.* **2024**, *52*, 141–152.
21. Yang, J.; Chen, Y.; Li, P.; Xu, C.; Zhang, M. Localized swelling-induced instability of tunnel-surrounding rock: Experimental and FLAC^{3D} simulation study. *Appl. Sci.* **2025**, *15*, 11101. [CrossRef]
22. Wu, F.; Dai, J.; Wen, Z.; Yao, C.; Shi, X.; Liang, L.; Yun, L.; Shi, B. Resistivity anisotropy analysis of Longmaxi shale by resistivity measurements, scanning electron microscope, and resistivity simulation. *J. Appl. Geophys.* **2022**, *203*, 104700. [CrossRef]
23. Li, C.; Wei, L.; Xu, Q.; Yang, L.; Li, J.; Wan, X. Structural detection and stability monitoring of deep strata on a slope using high-density resistivity method and FBG strain sensors. *Appl. Sci.* **2024**, *14*, 3272. [CrossRef]

Disclaimer/Publisher's Note: The statements, opinions and data contained in all publications are solely those of the individual author(s) and contributor(s) and not of MDPI and/or the editor(s). MDPI and/or the editor(s) disclaim responsibility for any injury to people or property resulting from any ideas, methods, instructions or products referred to in the content.